Key Engineering Materials
ISSN: 1662-9795, Vol. 395, pp 55-68
doi:10.4028/www.scientific.net/KEM.395.55
Online: 2008-10-21

Mechanical, Thermal, and Oxidation Behaviour of Zirconium Diboride Based Ultra-high Temperature Ceramic Composites

R. Mitra[1,a], S. Upender[1,b], M. Mallik[1,c], S. Chakraborty[1,d], and K.K. Ray[1,e]

[1]Departmemt of Metallurgical and Materials Engineering, Indian Institute of Technology, Kharagpur -721302, West Bengal, INDIA

[a]rahul@metal.iitkgp.ernet.in, [b]upender.sunkari@gmail.com, [c]manabmallik@yahoo.co.in, [d]subrata_1980@rediffmail.com, [e]kkrmt@metal.iitkgp.ernet.in

Keywords: Zirconium Diboride, Ultra high temperature ceramic composites, Mechanical Property, Thermal Shock, Ablation Resistance, Oxidation Resistance.

Abstract. A comparative study has been carried out on the mechanical properties at room temperature, thermal shock and ablation resistance as well as oxidation behaviour of ZrB_2-20SiC, ZrB_2-20SiC-5Si_3N_4 and ZrB_2-20ZrC-20SiC-5Si_3N_4 (amounts represent volume percent) composites. Fracture toughness has been determined using either three-point bend tests on single edge notch bend specimens, or by indentation technique. Addition of Si_3N_4 as sintering aid leads to enhancement in flexural strength and fracture toughness in the composite without ZrC. The specimens were subjected to thermal shock by quenching from temperatures in the range of 800°-1200°C to ice cold water, and to ablation by exposure to oxy-acetylene flame at 2200°C. The composite having ZrC as constituent, exhibits the highest resistance to damage due to thermal shock and ablation, while the ZrB_2-SiC composite shows the least change in mass during ablation. On the other hand, thermogravimetric experiments from room temperature to 1300°C have shown that the presence of ZrC is detrimental for oxidation resistance. Hence, the constituents of the composites need to be selected on the basis of the nature of application. The results of this study show that the investigated ZrB_2 based composites bear the potential for multiple use thermal protection of re-entry type space vehicles.

Introduction

The hypersonic vehicles usually have sharp leading edges and nose cones to allow maneuverability at high velocities. The leading edges and nose cones are subjected to large aero-thermal heating, which may raise the temperatures beyond 2000°C during re-entry, and consequently the materials used for these components require severe thermal protection. Refractory zirconium diboride composites belong to the class of ultra high temperature ceramics (UHTCs) due to their high melting points exceeding 3200°C and strength retention capabilities at elevated temperatures. The UHTCs based on zirconium diboride based composites have attracted strong research interest also due to their high temperature ablation and oxidation resistance, high refractoriness, high thermal conductivity and good thermal shock resistance [1,2]. Hence, the zirconium diboride based composites are candidate materials for the thermal protection tiles of sharp leading edges and nose-cones of the hypersonic vehicles.

ZrB_2 is of particular interest because of its moderate density (6.09 $g.cm^{-3}$) and ability to maintain yield strength of 125 MPa at 1800°C. The density of ZrB_2 is lower than that of niobium-based refractory alloys normally used in aerospace structural applications, requiring thermal protection against ablation and oxidation. However, past research results [2] show that the properties of ZrB_2 based composites are strongly dependent on processing. Lack of adequate oxidation resistance at high temperature has been cited as the major deterrence for the widespread use of ZrB_2 [3]. The mechanical, thermal, and oxidation properties of the zirconium diborides, carbides and their composites with SiC reinforcements have been evaluated by Opeka et al. [4] and Monteverde [5]. The addition of SiC as reinforcement to ZrB_2 improves the oxidation resistance, thermal shock resistance, flexural strength, and fracture toughness [6-9]. The SiC additions also aid in processing of the materials by reducing the maximum temperature required to densify the materials, and by reducing the growth of the ZrB_2 grains [10]. Further reduction in the sintering temperature is achieved by addition of Si_3N_4 as reinforcement, which aids in densification through removal of B_2O_3 from the surface of ZrB_2 particles [11]. Other related studies have shown that the hot pressed ZrB_2-ZrC-SiC based composites exhibit excellent ablation resistance [12,13].

The present study is focused on the microstructure, mechanical properties, thermal shock and ablation resistance, as well as isothermal and non-isothermal oxidation behaviour of the hot pressed ZrB_2 based composites. The role of Si_3N_4 and ZrC additions on the mechanical and oxidation behaviour of the ZrB_2-SiC composite has been examined.

Experiments, Results and Discussions

Experimental Procedure. The experiments carried out in this study are classified as: (i) Raw Materials and Processing; and (ii) Characterization.

Raw Materials and Processing. The powders of ZrB_2, ZrC, SiC, and Si_3N_4, were obtained from H.C. Starck, Germany. The average sizes of the ZrB_2, ZrC, SiC, and Si_3N_4 powder particles are 5.4 ± 2.2 μm, 4.8 ± 1.7 μm, 4.0 ± 1.4 μm, and 3.3 ± 1.1 μm, respectively. The purity of the powders was 99.5% or better. The powder samples of ZrB_2-20 vol% SiC (henceforth referred as ZS), ZrB_2–20 vol% SiC–5 vol% Si_3N_4 (ZSS), and ZrB_2–20 vol% ZrC – 20 vol% SiC–5 vol% Si_3N_4 (ZZSS) were mixed at a milling speed of 250 rpm for 2 h in the Planetary Mono Mill (model Pulverisette 6, Fritsch, Germany). The powders were wrapped in grafoil, placed in a cylindrical graphite die, and subsequently hot pressed in vacuum at 2000°C for 30 min using a uniaxial pressure of 30 MPa, into pancakes of 42 mm diameter.

Characterization. The hot pressed pancakes were sectioned using an Isomet slow speed diamond saw cutter (Buehler Ltd, USA). The sectioned samples were metallographically polished, and the microstructures were examined using secondary (SE) and backscattered (BSE) electron imaging modes on a JEOL JSM 5800 scanning electron microscope (SEM) to examine the distribution of the constituent phases, the chemical compositions of which were determined using Energy Dispersive X-Ray (EDX) analysis. X-ray diffraction (XRD) using Cu K_α radiation was used to identify the phases present. The densities of the hot pressed products were measured using the Archimedes principle with water as the immersing medium.

The elastic modulus of the composites was measured using the dynamic elastic property analyzer involving vibration of the sample with natural frequency [14]. The measurement of hardness was carried out using a Vickers diamond indenter operated with loads of 20 and 30 kg. Fracture toughness of the hot pressed composites was determined by three point bend testing of single edge notch bend (SENB) specimens, following the ASTM E399 standard procedure [15]. The SENB specimens having dimensions of 4 mm (thickness) X 8 mm (width) X 36 mm (length), and ~ 4 mm deep notch along the width were tested with a crosshead speed of 0.1 mm per min on a three point bend fixture with a span of 32 mm. The notches were cut using 0.3 mm thick diamond saw. The fracture toughness, K_{1C} was determined using the equation (1):

$$K_{IC} = [3PS/BW^{1.5}].f\,(a/W). \qquad (1)$$

where P is the load, S is the span, B is the thickness, W is the width, a is the initial crack length, and $f(a/W) = 3(a/W)^{0.5}/[2\{1+(2a/W)\}\{1-(a/W)\}^{1.5}\{1.99-(a/W)(1-a/W)(2.15-3.93a/W+2.7a^2/W^2)\}]$. Further, three-point bend tests were carried out at a crosshead speed of 0.1 mm per minute, using a fixture with 40 mm span, on specimens with dimensions of 3 mm (thickness) X 4 mm (width) X 42 mm (length) to determine the flexural strength following the procedure described in ASTM C 1161-94 [16]. The flexural strength, σ has been calculated using the equation (2):

$$\sigma = 3PS/2WB^2. \tag{2}$$

Selected samples of the investigated composites were subjected to thermal shock by heating at three different temperatures including 800°, 1000°, and 1200°C in air inside a vertical chamber furnace having SiC heating elements, and subsequently quenched in water. The damage to thermal shock was assessed quantitatively through the examination of changes in hardness, extension of indentation crack lengths, and indentation fracture toughness (IFT) of the composite samples after subjecting to thermal cycling. The IFT was measured using the empirical relationship provided by Niihara et al. [17]:

$$K_{IC} = 0.0309(E/H)^{0.4}(P/c^{1.5}) \tag{3}$$

where E is the Young's modulus, H is the hardness, P is the load, and c is the characteristic crack length. The lengths of the cracks at corners of indentations were measured before and after the thermal cycle to determine the changes in indentation fracture toughness. The procedure followed is somewhat similar to that used for the evaluation of thermal shock resistance of the ceramics and ceramic matrix composites in previous studies [18-20].

Ablation resistance was studied on the specimens having the dimensions of 6 mm (width) X 3 mm (thickness) X 30 mm (length). A neutral oxyacetylene flame with maximum temperature of 2200°C was employed to evaluate the ablation behavior of the samples, after exposures for 5, 10, and 15 min, respectively. An optical pyrometer and a thermocouple were used measure and record the time-temperature data of the front and the unattacked back surface of the specimens. The experimental set-up for the ablation experiment was designed on the basis of the procedure discussed in Refs. 12 and 13. Furthermore, the extent of damage was quantified in terms of the changes in mass, Young's modulus and indentation fracture toughness. X-Ray diffraction (XRD), followed by energy dispersive X-ray analyses on SEM was used to identify the oxide phases present after exposure.

Finally, non-isothermal oxidation behaviour of the composites has been studied by heating at the rate of 5°C/min in a Thermo-gravimetric (TG) Analyzer (Perkin Elmer, USA). The change in mass with increase in temperature has been measured using the dry, inert Al_2O_3 powder as reference.

Results and Discussion. The densities of the ZS, ZSS, and ZZSS composites have been found to be 5.50, 5.33, and 5.47 $g.cm^{-3}$, respectively, which are 99-100% of the theoretical values calculated from the rule of mixtures. The results of the experiments related to microstructural examination, mechanical and thermal property evaluation, as well as characterization of the resistance to oxidation, thermal shock and ablation, have been discussed separately in the sections below. Based on the results, an effort has been made to correlate the material properties with the structure and composition of the different UHTCs.

Microstructure. The microstructures of the ZS, ZSS, and ZZSS composites are shown in Figs. 1(a-c), respectively, and typical XRD pattern from the ZSS composite is shown in Fig. 2. The SEM images [Figs. 1(a-c)] clearly show a uniform distribution of phases in the microstructure. The ZrB_2 and ZrC phases appear bright, while the SiC and Si_3N_4 look dark. The identity of the major elements in each of these constituents has been confirmed by EDX analysis. Examination of the composition of the dark regions located at the grain boundary triple points, using EDX has shown evidence of Si and N enrichment. In a previous study on the ZrB_2-Si_3N_4 composites, it has been shown that the B_2O_3 present as impurity in the ZrB_2 is reduced by reaction with Si_3N_4 at around 1550°C during processing, and a liquid phase is formed, particularly at the grain boundary triple points. Such a reaction leads to the formation of BN and borosilicate type glass [11]. In the present study, the results of XRD analysis (Fig. 2) have shown the presence of Si_3N_4, which suggests that it exists and is possibly consumed only partially by chemical reaction during hot pressing.

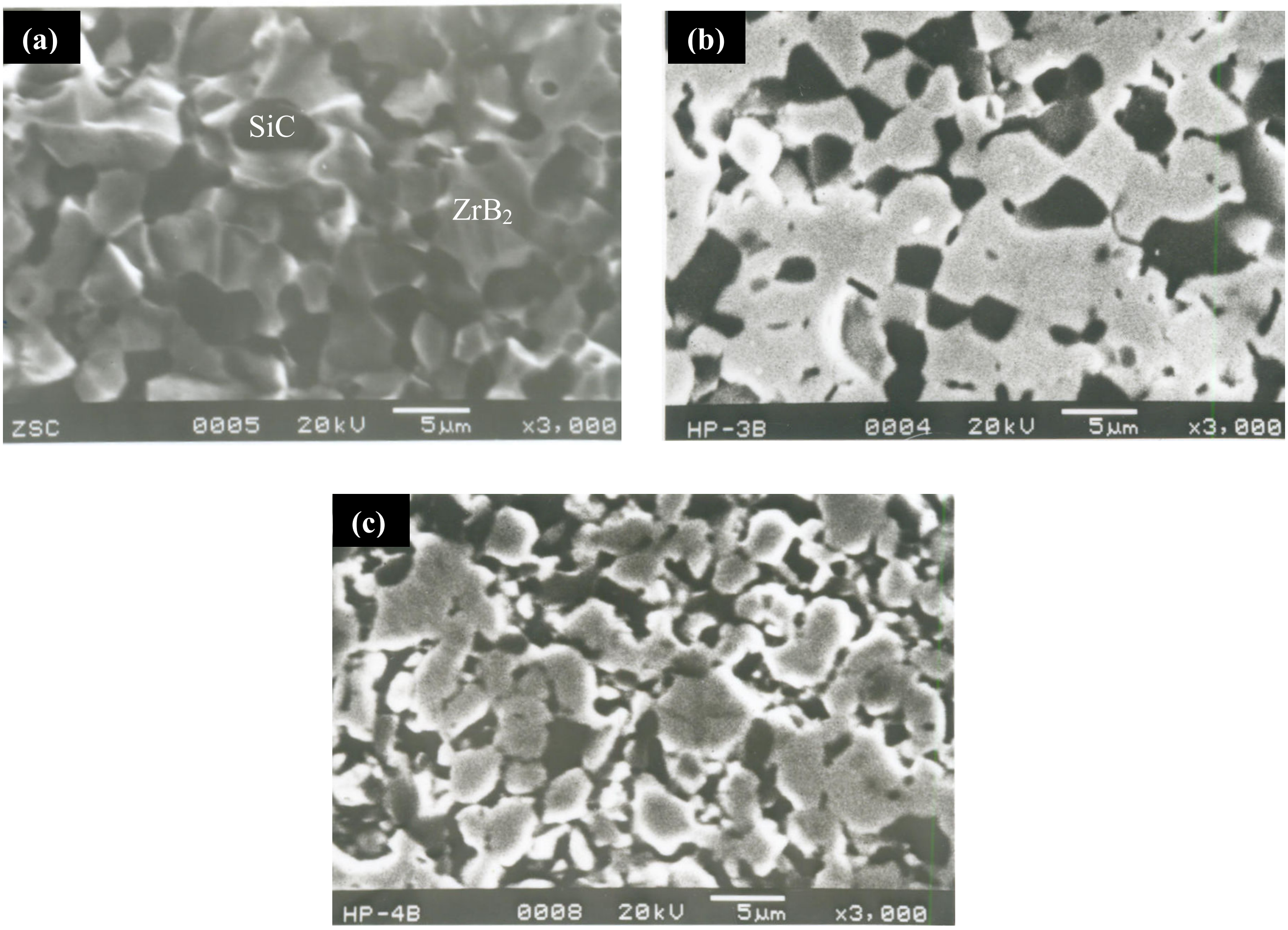

Fig. 1. SEM (SE) images showing the microstructures of: (a) ZS; (b) ZSS; and (c) ZZSS composites.

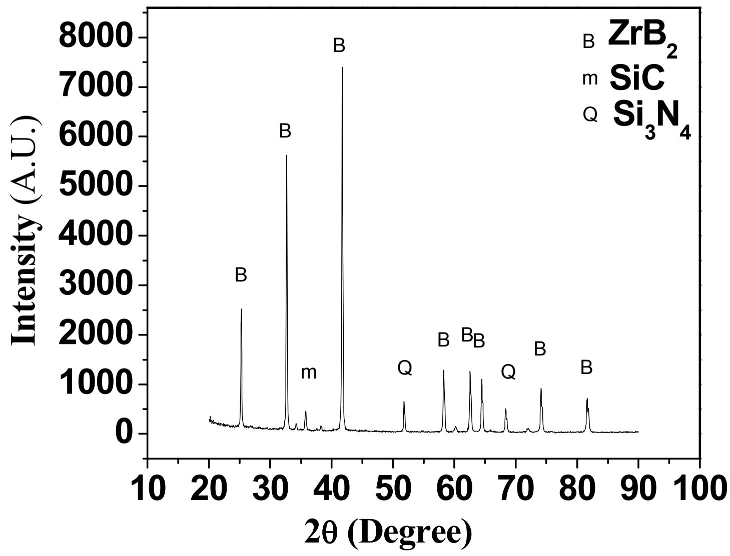

Fig. 2. XRD pattern from the ZSS composite showing the peaks of ZrB_2, SiC and Si_3N_4.

Mechanical Properties. The elastic modulus, hardness, flexural strength and fracture toughness of the investigated composites and those of monolithic ZrB_2 [21] for the purpose of comparison, are shown in the Table 1. The elastic moduli of the composites, calculated using the rule of mixtures, are also shown in Table 1 for comparison with the experimentally determined values. The experimentally determined Young's modulus has been compared with the values predicted by the rule of mixtures in some of the previous studies [22-24] on composites, for assessing the strength and integrity of the particle-matrix interfacial bond. A comparison of the experimental values of elastic modulus (E_{EXP}) with those predicted by the rule of mixtures (E_{ROM}) shows the E_{EXP} / E_{ROM} ratio to be close to 1, which suggests excellent bond integrity between the matrix and the reinforcement in case of the ZS and ZSS composites. However, the ratio of the experimentally determined Young's modulus to that from the rule of mixtures is the least in case of the ZZSS composites, suggesting that interfacial bonding between the ZrC and the other phases present is not as strong as that in the ZS and ZSS composites. The elastic modulus of the ZS composite with higher volume fraction of ZrB_2, is higher than those of the ZSS and ZZSS. The Young's modulus phase of ZrB_2 is higher than those of ZrC and Si_3N_4.

On examination of the data presented in Table 1, it is clear that the ZSS composite possesses the highest values of hardness (21.2 GPa), flexural strength (520 MPa) and fracture toughness (7.8 ± 0.6 MPa√m). Again, the improvement in fracture toughness with respect to that of monolithic ZrB_2 is the most significant in case of the ZSS composite (Table 1). The fracture toughness of the ZS, ZSS and ZZSS composites are higher than that of the monolithic ZrB_2 by 56%, 111%, and 27%, respectively. Figs. 2(a-c) show the typical fractographs, representing the respective fracture surfaces of the ZS, ZSS, and ZZSS composites, generated through flexural tests. The fractograph of the ZS composite, depicted in Fig. 2(a), suggests a mixed intergranular and transgranular mode of failure. The features suggesting transgranular failure include grain facets and river patterns. Transgranular failure is observed in the coarser grains, while the locations containing finer grains show evidence of intergranular failure [Fig. 3(a)]. In a previous study [25] based on fracture behavior of Al_2O_3, it has been shown that anisotropic ceramics with fine grain size tend to exhibit primarily intergranular failure, while the transgranular mode becomes predominant with increase in the grain size. A close examination of the fracture surface [Fig. 3(a)] also indicates that the ZS composite has a wide distribution of grain sizes, which is primarily responsible for the variation observed in the mode of failure. In contrast, the fracture surfaces [Figs. 3(b) and (c)] of the ZSS and the ZZSS composites are primarily intergranular. The average size of the grains appears to be between 2 and 4 μm. The grain size distribution appears to be the most homogeneous in the ZSS composite. The observation of intergranular fracture surface for the finer and more uniform grain size is consistent with the observations recorded for the ZS composite. The higher hardness, flexural strength and fracture toughness of the ZSS composite is attributed to its finer and more or less uniform matrix grain size. It may be noted that the volume fraction of SiC and Si_3N_4 are exactly same in the ZSS and ZZSS composites. The lower hardness and flexural strength of the ZZSS is composite is in spite of the high hardness and flexural strength reported for ZrC [26,27]. The lower than expected hardness and flexural strength of the ZZSS composite can perhaps be explained on the basis of inadequate interphase interfacial bond-integrity, as suggested by somewhat lower value of the Young's modulus of the composite than that predicted by the ROM (Table 1). However the values of hardness and fracture toughness of the ZZSS composite are in agreement with those reported for the ZrB_2-ZrC composites prepared by spark plasma sintering [28].

Table 1. Room temperature mechanical properties of the composites. *The abbreviation "ROM" stands for "Rule of Mixtures". The data for ZrB_2 is from Ref. 21.

Material	Young's modulus (GPa)	*ROM Young's modulus (GPa)	Hardness (GPa)	Flexural Strength (MPa)	Fracture Toughness (MPa√m)
ZrB_2	490	----	21.0	480	3.7
ZS	484	489	19.4	356	5.8 ± 0.2
ZSS	467	478	21.2	520	7.8 ± 0.6
ZZSS	427	447	17.5	407	4.7 ± 0.2

Thermal Shock Resistance. The hardness, change in the indentation crack length, and IFT measured before and after each thermal cycle experiment, are depicted through bar charts in Figs. 3(a-c), respectively. The hardness of all the composites decreases with increasing temperature drop (ΔT) during the thermal cycle [Fig. 4(a)]. But the rate of decrease in hardness of the ZZSS composite is lower than that of ZS and ZSS. The change in indentation crack length, $\%\Delta c$ [$\%\Delta c = (c_f - c_i) \times 100/c_i$, where c_i and c_f are the respective crack lengths of samples before and after the thermal cycle] with ΔT is shown in Fig. 4(b). It can be seen that the $\%\Delta c$ increases continuously with increasing ΔT for all the composites. After thermal cycle, several micro-cracks are generated inside the composites. The cracks emanating from the tip of hardness indentation, link with the micro-cracks during its propagation, which in turn contribute to the extension in crack length. This may be considered as the reason for increase in $\%\Delta c$ with increase in ΔT. It is also intuitive that the micro-cracks are responsible for the degradation of hardness in the composites, subjected to temperature drop. The values of IFT are also found to degrade with increasing ΔT, as shown in Fig. 4(c). In the damaged specimens with micro-cracks, the flaw size is large and hence the critical stress intensity factor responsible for crack propagation is decreased significantly. This stress intensity factor gets superimposed with the stress intensity factor of the advancing long crack front from the indentation tip, which results in a higher crack length and in turn lowers the IFT.

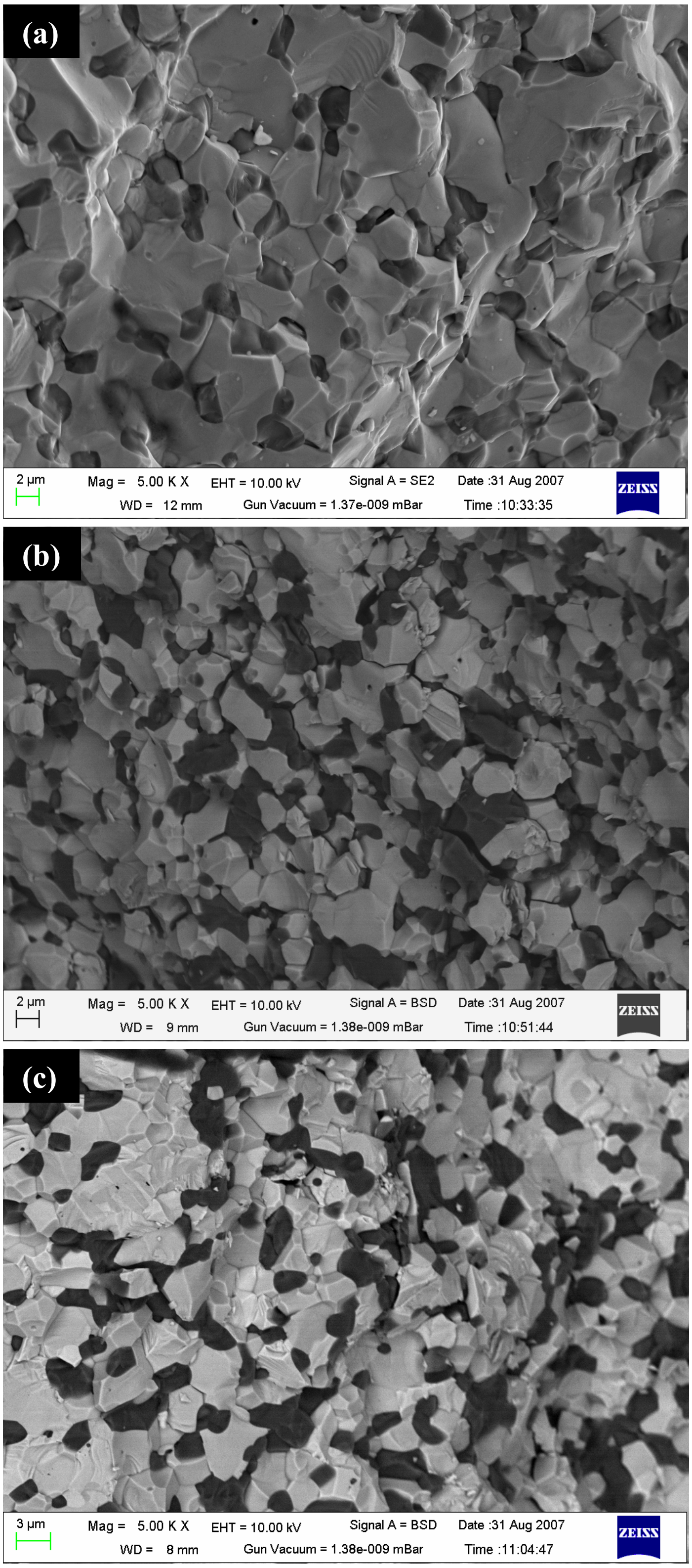

Fig. 3. Fracture surfaces of: (a) ZS; (b) ZSS; and (c) ZZSS composite. The ZrB_2 and ZrC appear bright, while the SiC and Si_3N_4 appear dark.

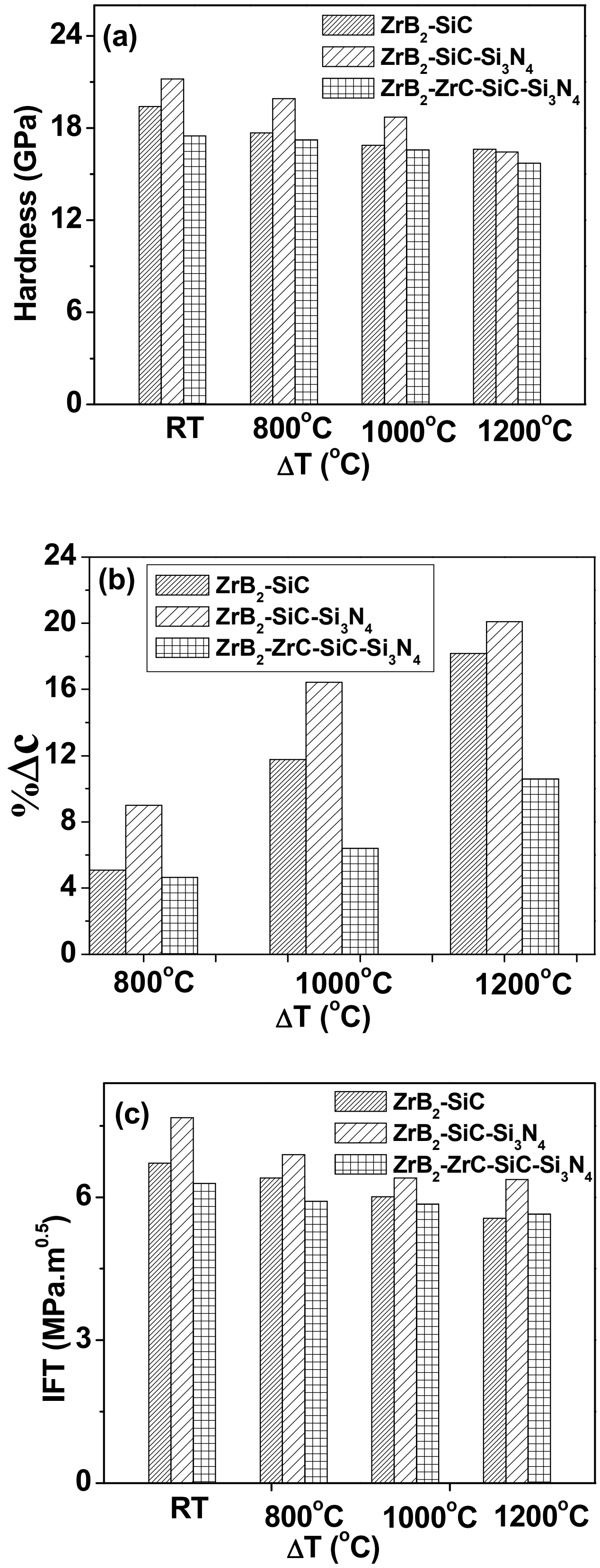

Fig. 4. Bar charts showing: (a) hardness, (b) indentation crack lengths and (c) values of the IFT, before and after thermal cycling between 800°, 1000°, or 1200°C and room temperature.

A comparison of the degradation behavior of the composites indicates that thermal shock resistance of the ZZSS composite (with ZrC) is superior to those of ZS and ZSS composites. This may be because of the marginal decrease in co-efficient of thermal expansion (CTE) of the matrix on addition of ZrC, and reduction in the mismatch between the constituent phases. The co-efficient of thermal expansion of ZrC is 5.5 x 10^{-6} K^{-1}, which is less than that of ZrB_2 (6.7 x 10^{-6} K^{-1}). Reduction in the CTE is expected to improve the thermal shock resistance of the composites.

Ablation Resistance. The front and back-face temperatures on the plates of the ZS, ZSS, and ZZSS composites have been recorded for 5, 10, and 15 min during heating with an oxy-acetylene flame. The typical pattern of the temperatures recorded on the front and back faces of the ZS composite during heating for 15 minutes, is depicted as time-temperature plots in Fig. 5. From examination of the results in Fig. 5, it is obvious that the front face is subjected to a temperature in the range of 2000^o-2200^{o}C, while the back face shows temperatures between 1200^o-1250^{o}C, during exposure to the oxy-acetylene flame. Thus, a temperature drop of about 800^{o}C across its thickness of 3 mm, is recorded. During the tests, the front face in each sample has taken about 200 s, while the back face has taken 100 s to reach the stable temperatures. It may be proposed that much of the heat generated due to the oxyacetylene flame is lost to the surroundings by radiation, and only a part is being conducted to the back surface.

The morphology of the front surfaces of the samples exposed to the oxy-acetylene flame for 15 min is depicted in the photograph presented in Fig. 6. Comparison of the surface characteristics clearly indicates that the oxide scale formed on the ZS composite has maintained its integrity, while there is evidence of spallation in case of the ZSS and ZZSS composites. The damage during ablation has been characterized in terms of the change in mass and Young's modulus. The change in mass per unit surface area due to high temperature exposure is shown using bar charts in Fig. 7. The bar charts indicate that all the composites have undergone a net gain in mass due to oxidation. It is clear that for a given time period of exposure, the ZS composite has shown the least gain in mass. On the other hand, the highest gain in mass after 5 min of exposure is observed in the ZZSS composite, while that after 10 and 15 min of exposure is observed in case of the ZSS composite. The elastic moduli and indentation fracture toughness values, before and after ablation for 10 min are shown using bar charts in Fig. 8(a) and (b), respectively. The drops in the Young's moduli, recorded after ablation of the ZS, ZSS, and ZZSS composites for 10 min, are 7.2, 8.4, and 3.3%, respectively [Fig. 8(a)]. Furthermore, ablation for 10 min has led to a noticeable decrease in the IFT of all the samples, that is, 20.8, 18.5, and 8.8% in case of the ZS, ZSS, and the ZZSS composites, respectively [Fig. 8(b)]. Comparison of the drops in Young's modulus and indentation fracture toughness clearly indicates that the decrease in modulus and indentation fracture toughness is the least in case of the ZZSS composite. Hence it can be inferred that among the investigated composites, internal damage due to ablation is minimum in the ZZSS composite, in spite of a high mass gain exhibited by it in the first 5 min of exposure to oxy-acetylene flame. The observation of the highest ablation resistance is in agreement with that in previous studies [12,13], and is attributed to the formation of a passivating oxide scale.

Figure 9 shows the typical XRD pattern from the ZSS composite surface after ablation for 10 min, showing the peaks of ZrB_2, ZrO_2, SiO_2 (cristobalite) and $ZrSiO_4$, formed by oxidation. Similar peaks are observed in the XRD patterns from the ablated surfaces of the ZS and ZZSS composites. The cross-section of the damaged sub-surface location and oxide scale formed on the ZSS composite due to exposure to the oxy-acetylene flame for 10 min is shown in Fig. 10. The affected zone appears to be 40-50 μm thick. Considering that the ZSS composite is the worst affected in terms of mass gain in case of exposure to the oxy-acetylene flame for 10 and 15 min, it may be proposed that the damage is superficial.

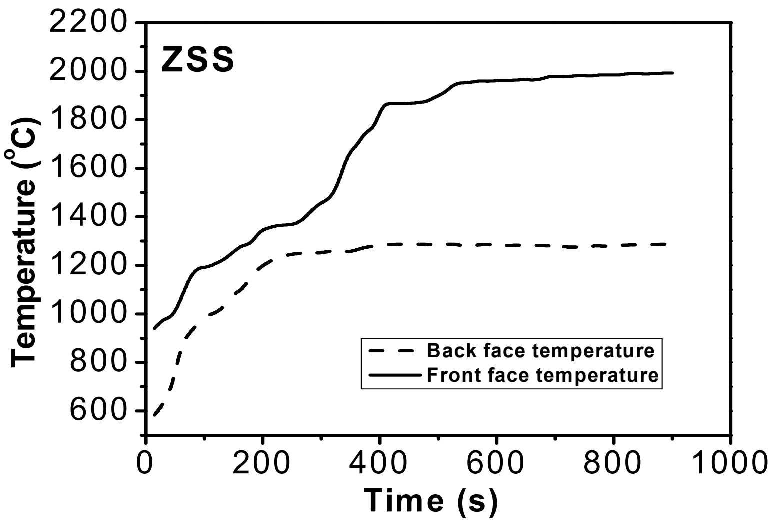

Fig. 5. Variation of the front and back face temperatures in the ZSS composite with time elapsed during the 15 min of exposure to the tip of the oxy-acetylene flame.

Fig. 6. Typical photograph of ZS, ZSS, and ZZSS composite specimens ablated for 15 min.

Oxidation Behaviour. Non-isothermal oxidation behavior studied using thermogravimetry (TG) of the ZS, ZSS, and ZZSS composites is depicted in Fig. 11. From the plots shown in Fig. 11, it is clear that the process of oxidation characterized by mass gain, is initiated at approximately 800^{o}C, followed by a much sharper rise at around 1200^{o}C in case of ZS, and ZSS composites. On the other hand, the ZZSS composite has shown gain in mass at a much lower temperature of 600^{o}C, with change in the mass gain characteristics at 800^{o}C. The net mass gains of the ZS and ZSS composites are almost identical, while that of the ZZSS composite is much higher. The ZZSS composite differs from the other two in having ZrC as a major constituent. Hence it can be inferred that the presence of ZrC in the ZZSS composite is primarily responsible for its poor oxidation resistance.

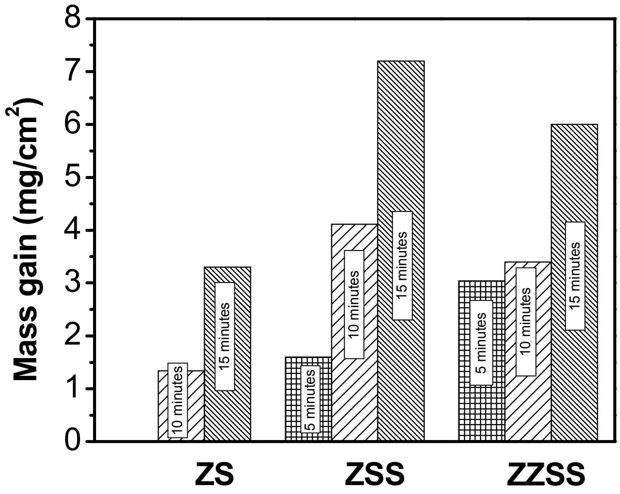

Fig. 7. Bar charts showing the mass gain per unit area of the ZS, ZSS, and the ZZSS composite during exposure to the oxy-acetylene flame for 10 min.

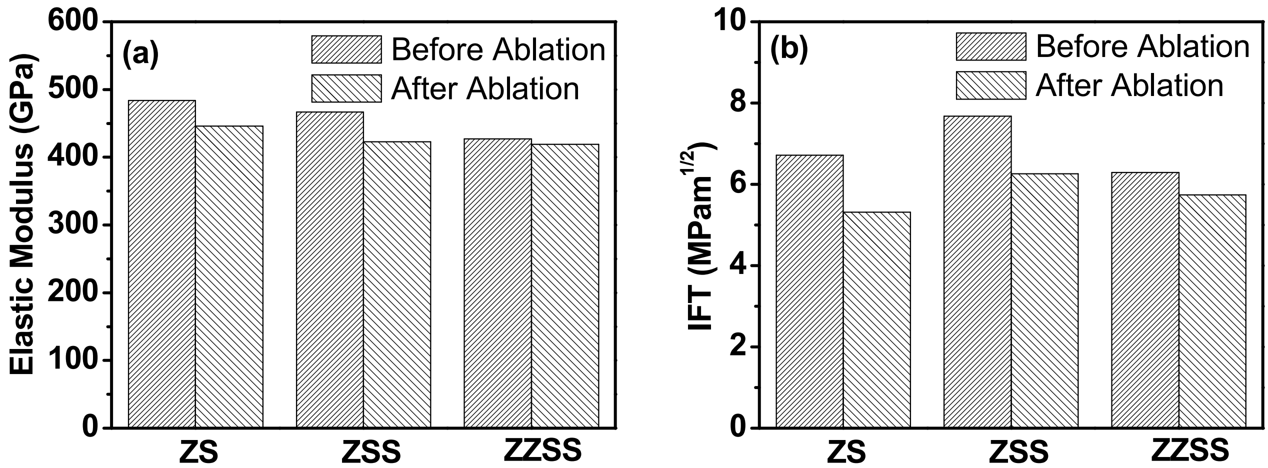

Fig. 8. Bar charts depicting: (a) elastic modulus, and (b) IFT of the ZS, ZSS, and the ZZSS composite before and after ablation for 10 min.

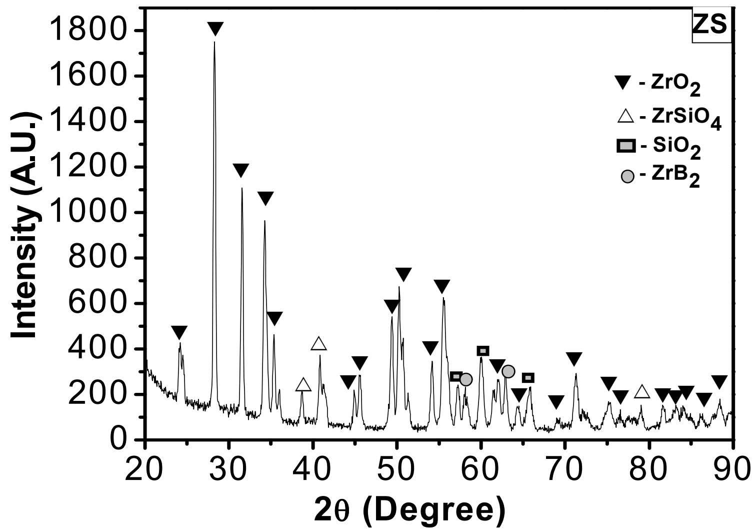

Fig. 9. Typical XRD pattern from the ZS composite surface after ablation for 10 min, showing the peaks of ZrB_2, ZrO_2, SiO_2 (cristobalite) and $ZrSiO_4$.

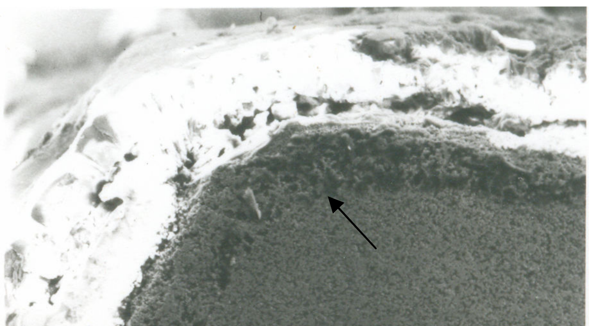

Fig. 10. SEM (SE) image showing the cross-section of the oxide scale formed on the ZSS composite during exposure to the tip of oxy-acetylene flame. The damaged region is shown with an arrow.

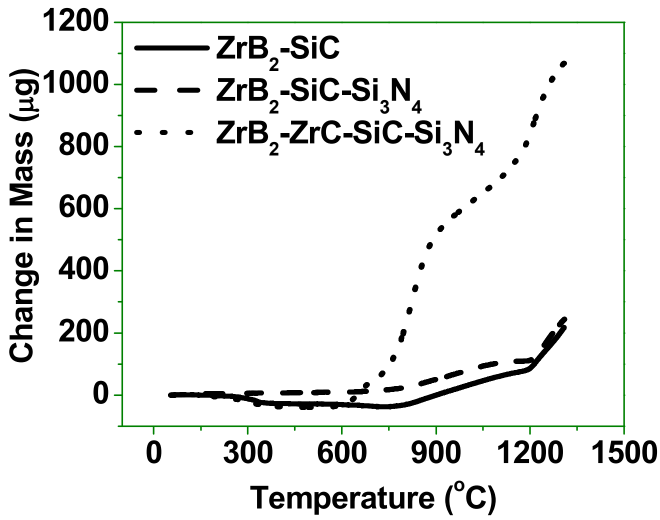

Fig. 11. Results of TG analyses: Plots showing the change in mass in the ZS, ZSS, and the ZZSS composites with temperature during heating.

Summary

ZrB_2-SiC (ZS), ZrB_2-SiC-Si_3N_4 (ZSS) and ZrB_2-ZrC-SiC-Si_3N_4 (ZZSS) composites with almost 100% of their theoretical densities, have been processed by hot pressing. The microstructures have shown a uniform distribution of the constituent phases with little porosity. The results of this study may be may be summarized as follows:

(1) Among the investigated composites, the ZSS has exhibited the most optimum combination of Young's modulus, hardness, fracture toughness and flexural strength.
(2) The fracture surfaces bear evidence of partial intergranular and transgranular failure, with the former being more predominant in case of the ZSS and ZZSS composites with finer and relatively uniform matrix (ZrB_2) grain size.
(3) Thermal shock resistance of the composites have been examined with temperature differentials of 800^o, 1000^o and 1200^{o}C, followed by measurements of Young's modulus, hardness, and extension of the indentation crack lengths, have shown the least damage in case of the ZZSS composites.
(4) Ablation studies have been carried out by exposure of the ZS, ZSS, and the ZZSS composites for periods of 5, 10, and 15 min to the oxy-acetylene flame. During the tests, the front face in each sample has taken about 200 s, while the back face has taken 100 s to reach stable temperatures in the range of 2100^o-2200^{o}C and 1200^o-1300^{o}C, respectively. In all the composites, a temperature drop of about 800^{o}C across the thickness of 3 mm was observed, irrespective of the time of exposure.
(5) Examination of the ablated front surfaces, and analysis of the damage using measurements of change in mass, Young's modulus, and indentation fracture toughness, have shown that the ZZSS composite is the least prone to internal damage, while the ZS composite is the most resistant to oxidation.
(6) Non-isothermal oxidation studies involving thermogravimetry, have shown that noticeable gain in mass is initiated in the ZZSS composite at 600^{o}C, and in the ZS and ZSS composites at 800^{o}C.

Acknowledgement

The financial support received from the Defence Research and Development Laboratory under CARS Contract No. DRDL/23/96P/05/0173/31454 is gratefully acknowledged.

References

[1] A. L. Chamberlain, W. G. Fahrenholtz, G. E. Hilmas, D. T. Ellerby: Key Eng. Mater. Vol. 264 (2004), p. 493.
[2] Federick Monteverde, Stefano Guicciardi and Alida Bellosi: Mater. Sci. Eng. Vol. A346 (2003), p. 310.
[3] Stanley R Levine, Elizabeth J. Opila, Michael C.Halbig, James D. Kiser, Mrityunjay Singh and Jonathan A. Salem: J. Eur. Ceram. Soc. Vol. 22 (2002), p. 2757.
[4] Mark M. Opeka, Inna G. Talmy, Eric. J. Wuchina, James A. Jaykoski, and Samuel J. Causey: J. Eur. Ceram. Soc. Vol.19 (1999), p. 2405.
[5] Federick Monteverde: Comp. Sci. Tech. Vol. 65(11-12) (2005), p.1869.
[6] W. G. Fahrenholtz, G. E. Hilmas, A. L. Chamberlain and J. W. Zimmermann: J. Mater. Sci. Vol. 39 (2004), p. 5951.
[7] Sumin Zhu, W.G. Fahrenholtz, G.E. Hilmas: J. Eur. Ceram. Soc. Vol. 27 (2007), p. 2077.
[8] Xinghong Zhang, Lin Xu, Shanyi Du, Jiecai Han, Ping Hu, Wenbo Han: Mater. Lett, in press.
[9] Alireza Rezaie, William G. Fahrenholtz, Gregory E. Hilmas, J. Eur. Ceram. Soc. Vol. 27 (2007), p. 2495.
[10] E. V. Clougherty, D. Kalish and E. T. Peters: Airforce Materials Laboratory Technical Report AFML-TR-68-190, Wright-Patterson Airforce Materials Laboratory, Dayton, OH, USA (1968).

[11] Federic Monteverde and Alida Bellosi: Scripta Mater. Vol. 46 (2002), p. 223.

[12] Jeffrey Bull, Michael J. White, and Larry Kaufman: US Patent 5,750,450. (1998)

[13] R. E. Loehman: Industrial Heating, January 11 (2004).

[14] ASTM C 1259-01, *Annual book of ASTM standards*, section 15, American Society for Testing and Materials, Philadelphia, PA, USA (2001).

[15] ASTM E 399-83, *Annual book of ASTM standards,* section 3, p. 500, American Society for Testing and Materials, Philadelphia, PA, USA (1990).

[16] ASTM C 1161-94, *Annual book of ASTM standards*, pp. 309-15, American Society for Testing and Materials, Philadelphia, PA, USA (1996).

[17] K. Nihara, R. Morena, D.P.H. Hasselman, in: *Brittle Matrix Composites* 2, R.C. Bradt, D.P.H. Hasselman, F.F. Lange (Eds.), Elsevier Applied Science, New York (1983), p. 84.

[18] G. Fargas, D. Casellas, L. Llanes, and M. Anglada: J. Eur. Ceram. Soc. Vol. 23 (2003), p. 107.

[19] Pernilla Petterson, Mats Johnsson: J. Eur. Ceram. Soc. Vol. 23 (2003), p. 309.

[20] ShuQin Li, Yong Huang, YongMing Luo, ChangAn Wang, CuiWei Li: Mater. Lett. Vol. 57 (2003), p. 1670.

[21] R. Telle, L. S . Sigl and K. Takagi, in: *Handbook of Ceramic Hard Materials*, edited by R. Riedel, Wiley-VCH, Weinheim (2000), p. 803.

[22] M.E. Fine: Scripta Metall. Vol. 15 (1981), p. 523.

[23] M.S. Zedalias, M.V. Ghate and M.E. Fine: Scripta Metall. Vol. 19 (1985), p. 647.

[24] R. Mitra and Y.R. Mahajan: Bull. Mater. Sci. Vol. 18(4) (1995), p. 405.

[25] P.L. Swanson, C.J. Fairbanks, B.R. Lawn, Y.-W. Mai, and B.J. Hockey: J. Am. Ceram. Soc., Vol. 70 (4) (1987), p. 279.

[26] Information available on http://www.azom.com/details.asp?ArticleID=261.

[27] Charles C. Sorrell, Vladimir S. Stubican, Richard C. Bradt: J. Am. Ceram. Soc., Vol. 69(4) (1986), p. 317.

[28] Tsuchida Takeshi, Yamamoto Satoshi: J. Mater. Sci., Vol. 42(3) (2007), p. 772.